Journal of Solid State Chemistry **145,** 716–730 (1999)
Article ID jssc.1999.8295, available online at http://www.idealibrary.com on IDEAL®

Synthesis and X-Ray Characterization of Silicon Clathrates

Ganesh K. Ramachandran,*,[1] Jianjun Dong,† Jason Diefenbacher,‡ Jan Gryko,§ Robert F. Marzke,† Otto F. Sankey,†,¶ and Paul F. McMillan*,¶

*Department of Chemistry and Biochemistry; †Department of Physics and Astronomy, ‡Science and Engineering of Materials Program; ¶Center for Solid State Science, Arizona State University, Tempe, Arizona 85287; §Department of Physical and Earth Sciences, Jacksonville State University, Alabama 36265

Received September 8, 1998; received in revised form March 17, 1999; accepted March 23, 1999

We report on the synthesis and characterization of two silicon clathrates, Na_8Si_{46} and Na_xSi_{136}($x = 4$–23), by powder X-ray diffraction, combined with Rietveld profile analysis. In Na_8Si_{46}, no deviation from the ideal stoichiometry is observed. In Na_xSi_{136}, systematic changes in X-ray diffraction intensities enable the Na content and site occupancy to be characterized. In the same structure, we observe a $\sim 0.5\%$ increase in the unit cell edge upon progressing from Na_4Si_{136} to $Na_{23}Si_{136}$. A statistical mechanical model, combined with experimental data for this phase reveals a preference for the removal of sodium from the smaller of the two available cages by 0.190 ± 0.050 eV. © 1999 Academic Press

INTRODUCTION

Considerable research has been focused on clathrate hydrates, structures which are formed when water molecules form cage-like structures around gas molecules or other solvent molecules. Naturally occurring isomorphs include the framework silicates melanophlogite and dodecasil-3C. Analogous open framework compounds consisting of 3D networks of tetrahedral silicon were first synthesized and characterized by Cros *et al*., in 1965 (1). Obtained as metastable phases during thermal decomposition in vacuum of the Zintl phase NaSi, which contains Na^+ and tetrahedral Si_4^{4-} ions, these structures were termed "clathrates," by analogy with the isostructural clathrate hydrate structures and because of the host–guest nature of the open silicon framework and the *endohedral* sodium (or other alkali/alkaline-earth) atoms. Although several structure types of clathrate hydrates [2] have been described, only the Structure I and Structure II silicon analogs of the clathrate hydrates have been observed to date. During decomposition of NaSi and volatilization of sodium into the vacuum, the tetrahedral silicon framework rearranges into one or both of these network structures, perhaps partly aided by the templating action of the remaining sodium atoms or ions. The silicon analog of the Structure I clathrate hydrate is the clathrate Na_ySi_{46} ($y = 8$ in this study) and Na_xSi_{136} ($0 < x < 24$) is the analog of the Structure II clathrate hydrate.

There is current interest in clathrate hydrates and other clathrate structures in potential applications such as molecular recognition, for encapsulation of specific atoms, for waste CO_2 sequestration, and for natural gas storage, among others (2). Interest in silicon clathrates have been rekindled in the last five years following the prediction that they might have bandgaps that are direct and larger than the semiconducting diamond phase of silicon (3) and also by observation of superconducting behavior in clathrate phases doped with barium atoms (4).

The structurally related carbon-based fullerenes, which contain 5 and 6 membered rings of sp^2 connected carbon atoms (in contrast the Si atoms are sp^3 bound in the clathrates) are known to become metallic and superconducting upon *interstitial* doping with alkali metals (5). The clathrate Na_xSi_{136}, shows an insulator-metal transition at $x \sim 11$ (6), and the mixed clathrate $Na_2Ba_6Si_{46}$ was found to become superconducting at ~ 4 K (4). More recently, phases of the formula $Ba_8M_xSi_{46-x}$ (M = Au, Ag, Cu) were shown to have superconducting critical temperatures in the range 5–6 K (7). Other interesting electronic properties, such the magnitudes of the Seebeck coefficients, as well as the relative stability of the silicon clathrates in air and moisture have led to the recent suggestion of potential applications of these materials in thermopower devices (8).

With the aim of better understanding the effect of alkali doping in the Na–Si clathrates, we have synthesized for the first time a systematic series of *phase pure* silicon clathrates Na_xSi_{136} ($x \approx 4$, 6, 7, 8, 10, 12, 13, 16, 18, 21, and 23). In this paper we report on our samples analyzed by powder X-ray diffraction combined with Rietveld profile analysis. A statistical mechanical model for the filling scheme in the non-stoichiometric Na_xSi_{136} phase is also described which enables a quantitative estimate for the difference in energy

[1]To whom correspondence should be addressed. E-mail: krg@asu.edu.

0022-4596/99 $30.00

between the two available cages. As part of this study the clathrate Na_8Si_{46} was also synthesized and characterized. The occupancy of the silicon framework in Na_8Si_{46} is of particular interest. In the related K–Sn and Rb–Sn compounds, Zhao and Corbett [9] have shown that the appropriate stoichiometries are K_8Sn_{44} and Rb_8Sn_{44}, with two tetrahedral vacancies per formula unit (i.e., $K_8Sn_{44}\square_2$). This formulation permits a rationalization of the electronic structure via simple electron counting schemes to give closed shell semiconducting compounds. In the present case, however, our X-ray structure refinement along with chemical analysis data confirm that the Na_8Si_{46} compound is fully stoichiometric, within analytical error. The resulting "additional" electrons occupy the conduction band, to give a metallic compound.

STRUCTURAL DETAILS

In the Na_8Si_{46} structure the silicon framework is made of two types of polyhedra, one with 20 silicon atoms (dodecahedra, Si_{20}; center at 2*a* sites) and the other with 24 silicon atoms (tetrakaidecahedra, Si_{24}; center at 6*d* sites). Two 20-atom cages and six 24-atom cages constitute an unit cell. The building blocks and the structure are depicted in Figs. 1 and 2, respectively. The structure has symmetry $Pm\bar{3}n$, and the unit cell edge *a* is ≈ 10.19 Å. The positions of the centers of the polyhedra, where the guest atoms reside, correspond to the positions of atoms in the Cr_3Si structure. The bond angles are close to the ideal tetrahedral angle ranging from 105.5° to 124.5°, the largest angle being the Si–Si–Si bond angle on the six membered rings defining the tetrakaidecahedra. Bond lengths of 2.36–2.37 Å are very similar to those in crystalline silicon (2.35 Å) as well.

In the Na_xSi_{136} $(0 < x < 24)$ structure there again are two types of polyhedra, one with 20 silicon atoms (dodecahedra, Si_{20}; center at 16*c* sites) and the other with 28 silicon atoms (hexakaidecahedra, Si_{28}; center at 8*b* sites). Sixteen 20-atom cages and eight 28-atom cages constitute an unit cell (Fig. 2). The structure crystallizes in the cubic $Fd\bar{3}m$ space group and is shown in Fig. 3. The positions of the centers of the polyhedra, where the guest atoms reside, correspond to the positions of atoms in the $MgCu_2$ structure. Bond lengths (2.34–2.40 Å) are again very similar to those in silicon. The bond angles range between 105.8° and 120.1°. The reader should note that a common motif in both clathrate structure is the presence of dodecahedral cages.

EXPERIMENTAL DETAILS

Sodium metal and ground silicon were mixed under argon in a tantalum capsule and sealed in a steel bomb and heated for 24 h at 650°C. The recovered "alloy" was then heated at 275°C under a vacuum of $\sim 10^{-6}$ Torr for 8 h to obtain the stoichiometric NaSi (sodium silicide). Aliquots of

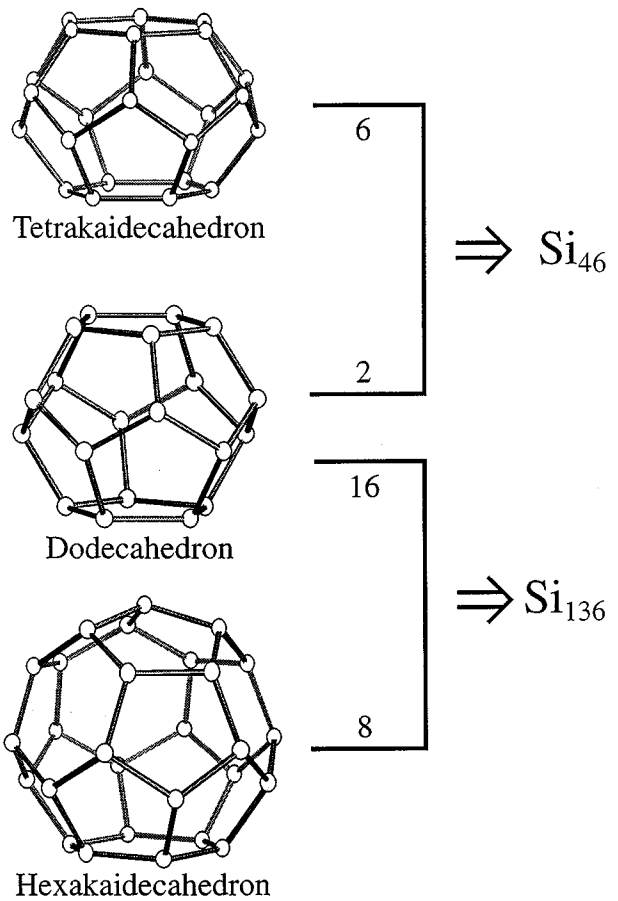

FIG. 1. Building blocks of Structure I and Structure II silicon analogs of clathrate hydrates. In the Si_{46} structure, which has a simple cubic structure, two smaller dodecahedra (Si_{20}) and six larger tetrakaidecahedra (Si_{24}) are fused together through 5-ring windows. In the Si_{136} structure, which crystallizes as a face centered cube, 16 smaller dodecahedra and eight larger hexakaidecahedra (Si_{28}) are fused together through 5-membered windows.

the silicide were placed in a tantalum boat and sealed in a quartz tube assembly so as to enable connection to a vacuum line. After establishing a vacuum of $\sim 10^{-6}$ Torr the assembly was heated to 375°C, within the temperature range at which the silicides are known to decompose to form the clathrates (1).

In order to produce samples with different sodium contents, heating times were varied between 30 min to several hours. Preliminary inspection of X-ray patterns of the resulting black powders showed that the products were mixtures of the two phases, Na_ySi_{46} (*y* was determined to be 8 in this study; see details below) and Na_xSi_{136}. Rietveld refinements showed that the latter phase slightly dominated the contribution by weight (55% w/w). With shorter heating times (< 2 h), the clathrate samples contained some undecomposed silicide, which was removed during washing with EtOH and water. Generally, shorter heating times also

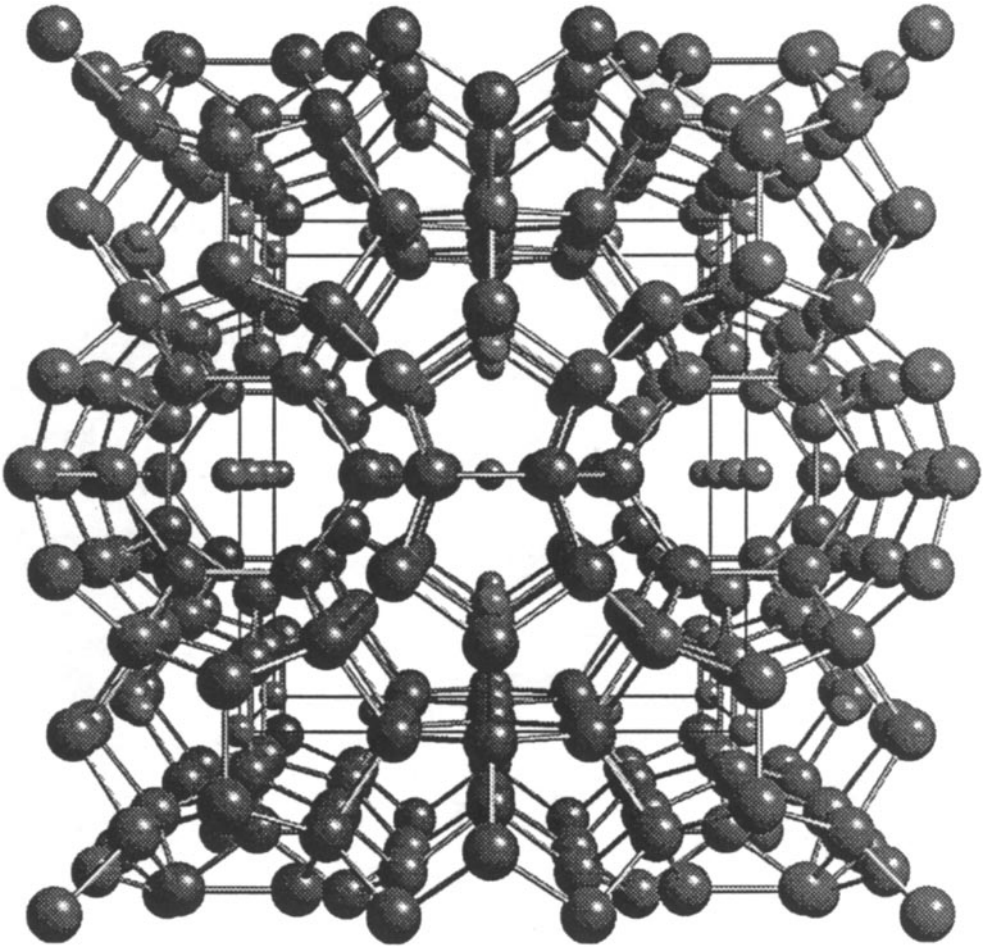

FIG. 2. The structure of Na_8Si_{46} shown along the [100] direction. Na_8Si_{46} is the Structure I analog of clathrate hydrates, for example $(CH_4)_8(H_2O)_{46}$. Other naturally occurring isomorphs include the framework of Melanophlogite. The larger tetrakaidecahedra form chains along [100] as in the β-W structure. The sodium atoms reside at the center of the cages and are shown as lighter small circles. In this study, the observed stoichiometry of this phase was Na_8Si_{46}.

resulted in the synthesis of the Na_xSi_{136} phase with larger sodium contents ($x > 12$ up to 23). We note that previous reports on synthesis of such samples required bathing of samples with $x < 11$ in sodium vapor (1, 10–11).

Phase fractions of the two phases and their densities were obtained from analysis of the X-ray patterns. Depending on x, the density of Na_xSi_{136} varied from ~ 2.33 g/cc to ~ 2.05 g/cc while samples of Na_ySi_{46} were found to have a constant density of 2.29 g/cc (implying that the sodium content in this phase did not change during heating). Solutions of dibromomethane ($\rho = 2.477$ g/cc) and tetrachloroethylene ($\rho = 1.614$ g/cc) were prepared in varying proportions to enable separation of the two clathrate phases employing a simple swim–sink procedure. After separation, the samples were washed with water and EtOH. The above procedure was repeated until essentially pure phases were obtained.

X-RAY CHARACTERIZATION

Powder X-ray patterns were collected on a Siemens D-5000 diffractometer at intervals of 0.02° from 2θ of 5° to 60° with a scan rate of 1°/min. This was followed by structure refinement of the X-ray data using the general structure analysis system (GSAS) software, a Rietveld profile analysis software developed by Larson and von Dreele [12]. Background coefficients, scale factor, peak shapes (with both Gaussian and Lorentzian contributions), atomic coordinates, until cell constants, phase fractions, thermal parameters, and site occupancies were all refined. The total sodium content in samples of Na_xSi_{136} and Na_8Si_{46} were obtained from the refined site occupancies and were independently confirmed by bulk density measurements and by electron microprobe analysis (Table 1).

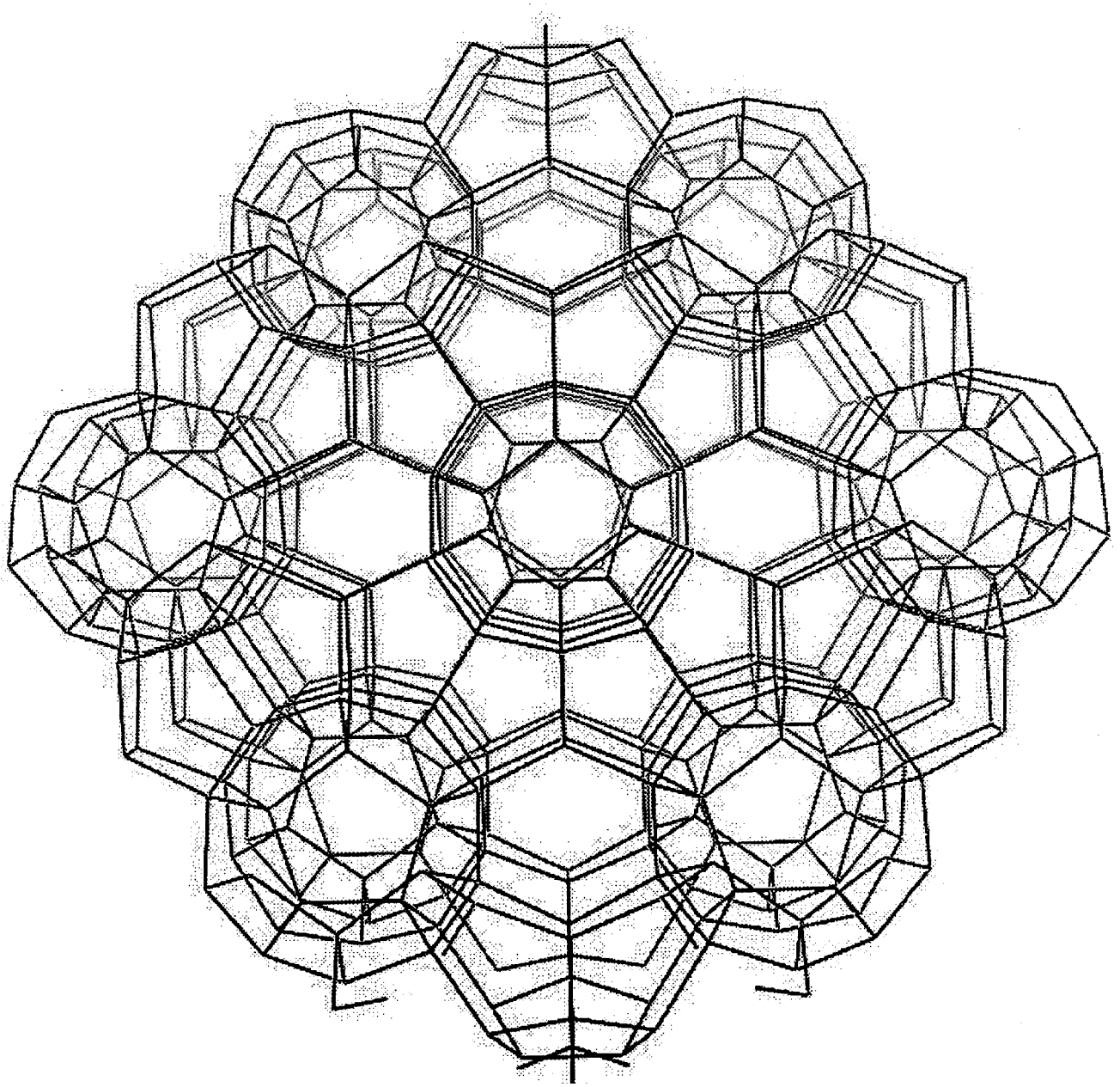

FIG. 3. A perspective of the Na_xSi_{136} structure shown along the [110] direction. Na_xSi_{136} is the Structure II analog of clathrate hydrates. Other naturally occurring isomorphs include the framework of Dodecasil-3C. The guest atoms reside at the center of the cages (not shown). When all the polyhedra are occupied, 24 guest atoms can be accommodated. In this study, we report on samples with sodium contents (x) varying between 4 and 23.

THE STRUCTURE I CLATHRATE Na_8Si_{46}

In Fig. 4 is shown the Rietveld profile fit for a sample of Na_8Si_{46}. As there can be strong interactions between site occupancies and atomic displacement (thermal) parameters, U_{iso}, data refinements were performed constraining U_{iso} for all silicon atoms to be the same. The final data are summarized in Table 2. Residuals, R_p and R_{wp} were 0.049 and 0.065, respectively. A similar refinement (see Table 5 of Supplementary Information) was also performed without imposing the above constraint. Within error, the results on the site occupancies from both refinements were virtually identical. From the site occupancies, the sodium content per unit cell was obtained to be 7.95 ± 0.02 (a value of 8 being the maximum). For the silicon atoms we obtain a total composition of 45.81 ± 0.05 atoms per unit cell. Combined

TABLE 1
Sodium Contents from X-Ray and Elemental analysis[a] for Select Samples

Sample	Na Content from X-ray analysis	Na content from elemental analysis
Na_8Si_{46}	7.952 ± 0.020	8.14 ± 1.07
Na_4Si_{136}	4.394 ± 0.033	4.75 ± 3.41
Na_8Si_{136}	7.737 ± 0.039	5.14 ± 3.62
$Na_{12}Si_{136}$	12.416 ± 0.017	12.60 ± 3.60
$Na_{20}Si_{136}$	20.360 ± 0.025	18.83 ± 3.93
$Na_{23}Si_{136}$	23.361 ± 0.018	23.80 ± 2.86

[a]Samples were mounted in epoxy and polished for electron microprobe analysis using a beam diameter of ~2 μm and a beam current of 20 nA with an accelerating voltage of 15 kV. Standards for silicon and sodium were elemental silicon and albite (Na-feldspar).

with our elemental analysis (Table 1) and refined site occupancies (Table 2) with essentially full occupancies of both sodium and silicon sites, it confirms that the composition of the Structure I silicon clathrate is best expressed as Na_8Si_{46}. Moreover, the unit cell edge and refined silicon and sodium site occupancies for Na_8Si_{46} are in excellent agreement with other studies on this phase (1, 11). Our refined unit cell edge is 10.19648(2) Å, within 0.02% of the value 10.1983(2) Å recently reported by Reny *et al.* (11). Further, our recent quantitative ^{29}Si MAS NMR study of Na_8Si_{46} shows three distinct resonances, whose integrated intensities are in the ratio of [6.51 ± 0.62]: [15.74 ± 0.30]: [23.76 ± 0.48], further corroborating the absence of silicon vacancies in the structure (13).

THE STRUCTURE II CLATHRATE Na_xSi_{136}

Within the Na_xSi_{136} clathrate series, full Rietveld analyses of the observed X-ray diffraction profiles were used to analyze the Na content and site occupancy, as well as phase purity. However, simple visual inspection of the experimental X-ray patterns could also provide a useful and rapid guide to these parameters, which we found invaluable during the course of this research. This point is demonstrated by considering the theoretical X-ray patterns for a range of Na contents and site-filling schemes depicted in Figs. 5 and 6.

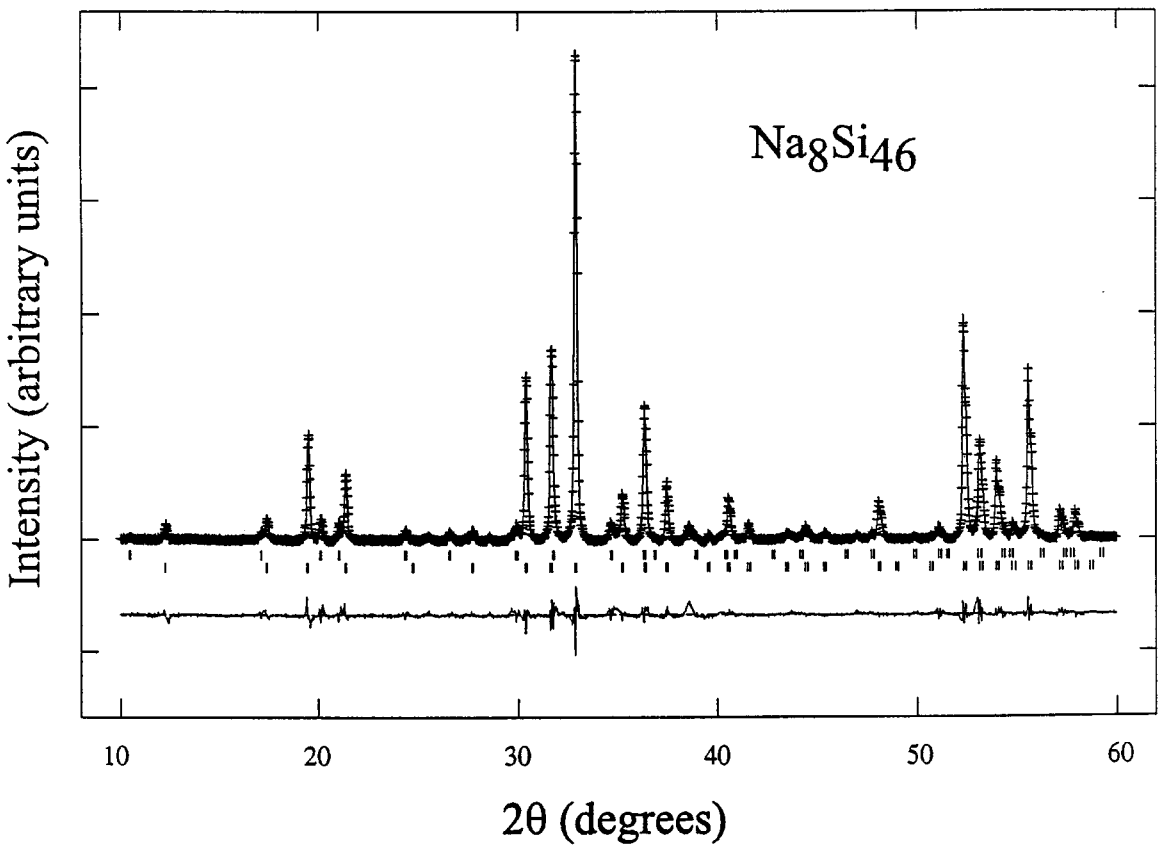

FIG. 4. Rietveld profile fit for Na_8Si_{46} (bottom tick marks). In order to check for purity, reflections for Na_xSi_{136} were also refined (top tick marks). Experimental data points are shown as plusses (+) and theoretical fits are shown as solid curves. Also shown below the fit is the difference between the observed and theoretical patterns. From the refined site occupancies, no nonstoichiometry was observed. See Table 2 for refinement details.

TABLE 2
Selected Refinement Details for Na_8Si_{46}

Space Group $Pm\bar{3}n$; $a = 10.19648(2)$ Å; $V = 1060$ Å^3
ρ_{bulk} and $\rho_{X\text{-ray}}$ 2.271 and 2.292 g/cc
Radiation wavelength Cu$K\alpha$ 1.5406 Å; 3288 data points
$\chi^2 = 2.57$; residuals (R_p[a] and R_{wp}[b]) 0.0499 and 0.0651
Elemental: Si 87.31 ± 1.76%, Na 12.69 ± 1.67%
Contained[c] ~ 2% Na_xSi_{136}

Atomic positions, site occupancies, and thermal displacement factors for Na_8Si_{46}

Atom	Site	x	y	z	Fraction	100 U_{iso} (Å^2)
Si3	6*c*	1/4	0	1/2	1.012(8)	0.476(2)
Si2	16*i*	0.1851(1)	0.1851(1)	0.1851(1)	0.997(7)	0.476(9)
Si1	24*k*	0	0.3077(2)	0.1175(2)	0.991(6)	0.476(9)
Na1	2*a*	0	0	0	1.009(8)	5.51(3)
Na2	6*d*	1/4	1/2	0	0.989(7)	3.49(4)

[a] $R_p = \sum |Y_{io} - Y_{ic}| / \sum Y_{io}$, where Y_{io} and Y_{ic} are the observed and calculated intensities at point i respectively;

[b] $R_{wp} = \{\sum w_i (Y_{io} - Y_{ic})^2 / \sum w_i Y_{io}^2\}^{1/2}$, where w_i is the weight assigned at each intensity step.

[c] Impurities here and in subsequent tables are expressed in w/w percentages.

In Fig. 5, we illustrate how the diffraction pattern varies as the total sodium content x varies from 0 to 24, assuming equal occupancy of both 20-atom (16*c* sites) and 28-atom (8*b* sites) cages. In Fig. 6 we show how the pattern changes for a fixed x ($x = 8$ was chosen) as the site occupancies are changed.

First, we focus on the relative intensities of the groups of peaks centered at 2θ of approximately 20° and 30°, as a function of total sodium content (assuming equal relative occupancies of the 8*b* and 16*c* sites, Fig. 5). As the sodium content is increased, the intensity of the 20° group of peaks is lowered relative to that at 30°, until the 30° group dominates the pattern for the fully loaded sample ($x = 24$).

In Fig. 6, we focus on the effect of relative occupancy of the two sites, for a given total sodium content ($x = 8$ as an example). We consider the three peaks at 2θ of approximately 18°, 20°, and 21°. As the relative population of the 8*b* sites increases, the relative intensity of the peak at 18° decreases and that at 21° increases. At the same time, the peak near 10° almost disappears. These systematic changes provide useful markers in interpreting the experimental spectra. These qualitative changes are made quantitative by refining the experimental spectra using Rietveld profile fits.

In Figs. 7–9 are shown the Rietveld refinements for samples with compositions close to Na_4Si_{136}, Na_8Si_{136}, $Na_{12}Si_{136}$, $Na_{16}Si_{136}$, $Na_{20}Si_{136}$, and $Na_{23}Si_{136}$. In Tables 3 and 4 (additional data can be seen in Supplementary Information) are summarized results from each of these refinements. The first noteworthy feature is a slight increase in the unit cell edge upon progressing from Na_4Si_{136} to $Na_{23}Si_{136}$ (Table 4, Fig. 10). The approximately linear dependence of a on x suggests that lattice parameters could be used as a rough convenient tool for analysis (Fig. 10). A similar report by Reny *et al.* (11) appeared at the completion of our work. As can be seen from Fig. 10, there is good agreement between the two data sets at the highest sodium contents, but not quite at the lowest sodium contents. It should be noted that in contrast to the present work, the compositions of Reny *et al.*, were determined from bulk, multiphase material. The X-ray diffraction patterns showed evidence of being amorphous in some instances at least, and it is likely that the true Na_xSi_{136} compositions were different from the bulk. Moreover, it was assumed that the 8*b* (larger, 16-hedral) sites filled completely before the 16*c* (smaller, 12-hedral) sites. Our results indicate that this is not quite the case; instead we find an energetic preference of 0.190 ± 0.05 eV for the occupation of 8*b* sites first. This is discussed in the following paragraphs.

We sketch in Fig. 11 the 8*b* and 16*c* site occupancies in Na_xSi_{136} as a function of the total sodium content. The data indicate that sodium atoms are removed preferentially from the smaller (16*c*) sites during heating. If we assume that the site distribution is in equilibrium at the experimental temperature during heating, a simple statistical mechanical model can reproduce this behavior with an energetic preference for Na atoms occupying the larger (8*b*) sites. The assumption that the filling scheme is in equilibrium is supported by the observation that similar site occupancy trends are obtained (i) in samples in which sodium atoms are removed from high sodium containing Na_xSi_{136}, (ii) in samples that are obtained directly in some instances, and (iii) in samples with large sodium contents reported in previous studies to have been made by treating samples of lower sodium contents with sodium vapor (10, 11).

First we define the total occupation number (y) as the ratio of total sodium content to the total number of available sites. Next we define the site occupancy of each of the sites as the ratio of the number of sodium atoms located at a particular site to the total number of sites of that type. We assume that there are N units of Si_{136} containing m_1 sodium atoms at the 8-site and m_2 atoms at the 16-site. The total occupation number is then $y = (m_1 + m_2)/24N$ and the site occupancies of the 8-site and 16-site are $y_1 = m_1/8N$ and $y_2 = m_2/16N$, respectively. We demand that the distribution of the sodium atoms is such that the total free energy (A) of the system is minimized; i.e., $A = U - TS$ such that $\delta A = 0$ with

$$U = m_1 \cdot E_{8b-\text{site}} + m_2 \cdot E_{16c-\text{site}},$$

$$S = k \ln W,$$

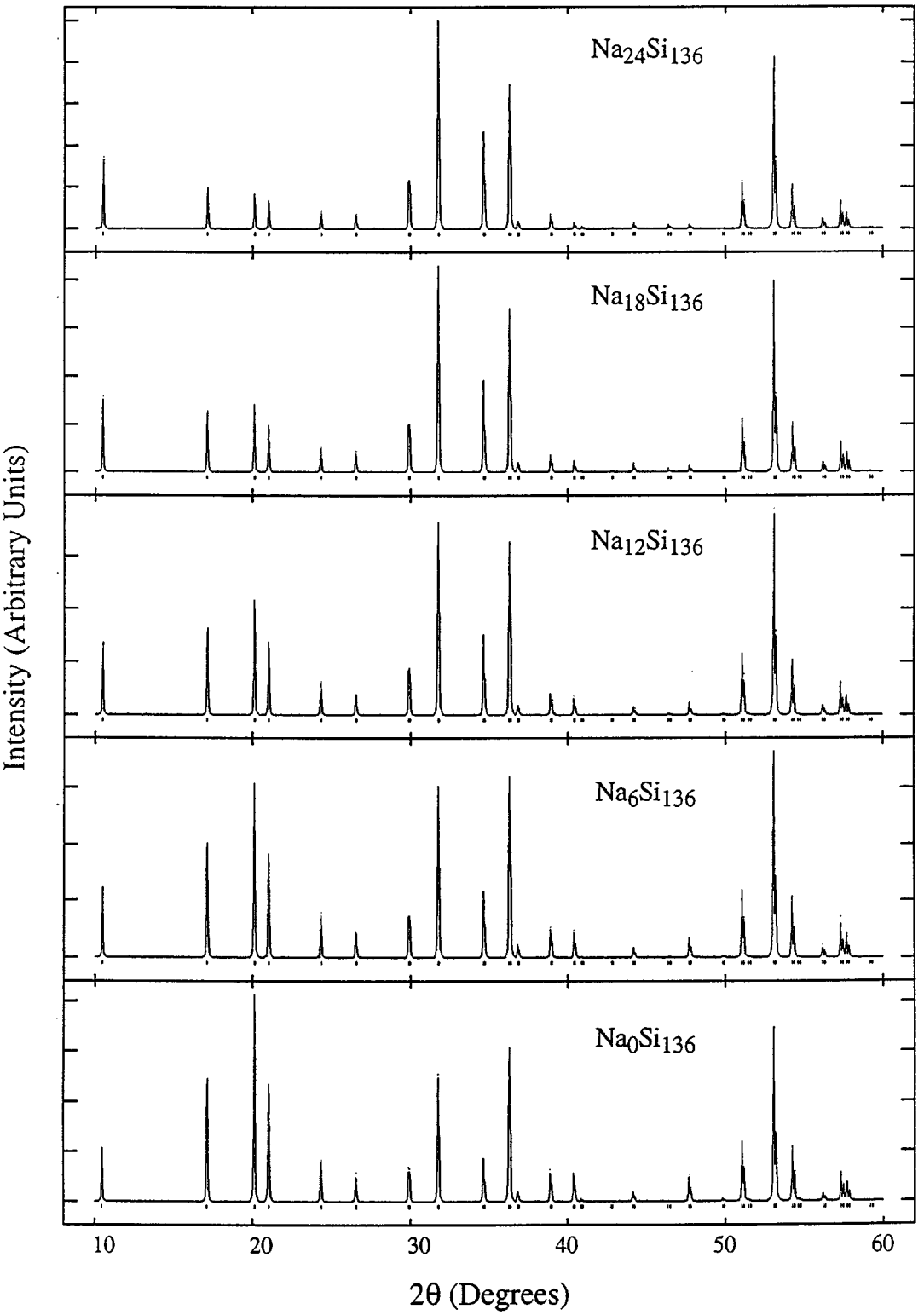

FIG. 5. The effect on X-ray peak intensities upon varying x in Na_xSi_{136}. Theoretical patterns are shown for different total sodium contents (x), keeping the occupancy of the two sites (8*b* and 16*c*) equal.

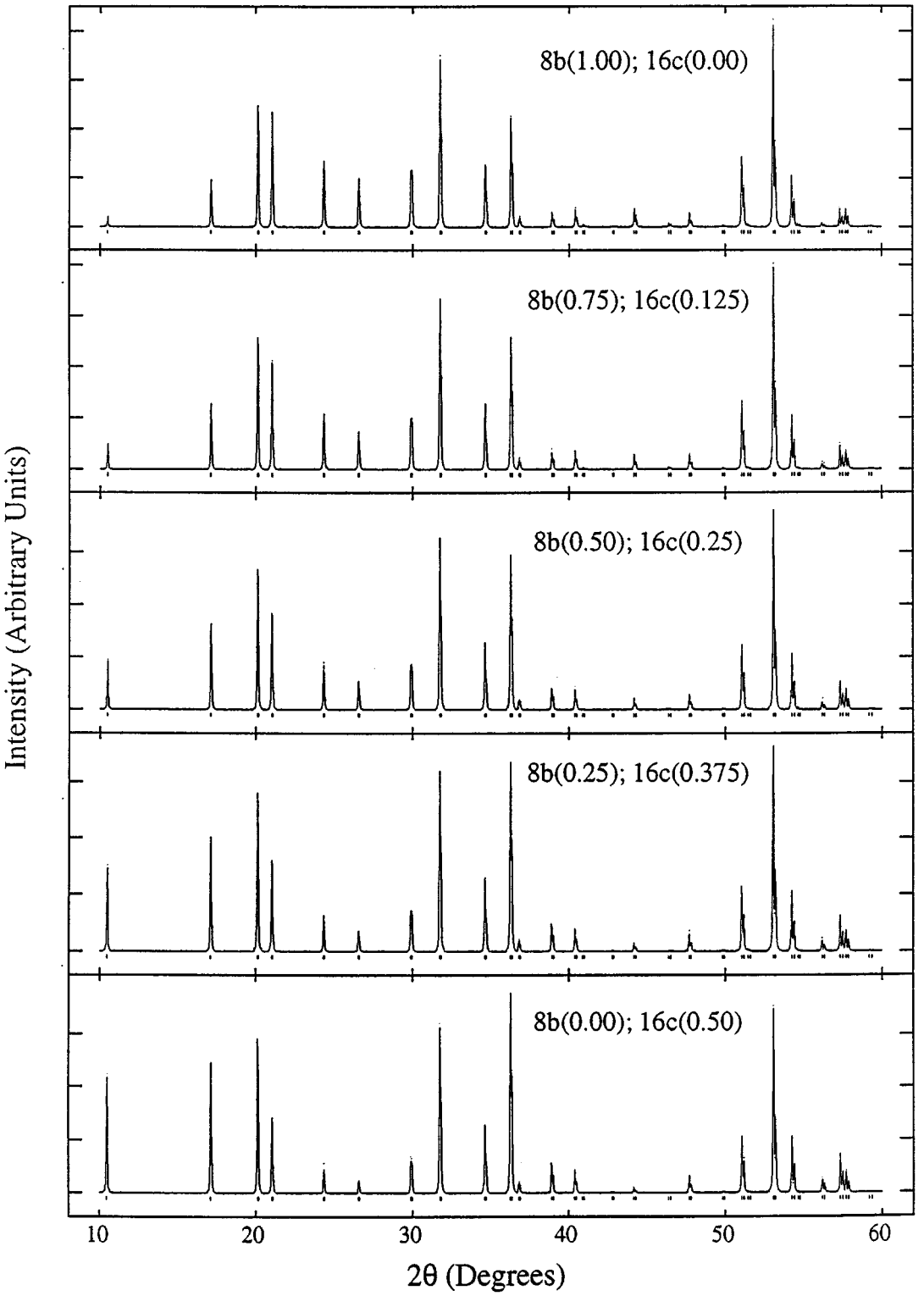

FIG. 6. The effect on X-ray peak intensities for Na_8Si_{136} upon changing the sodium occupancy in the two sites (8*b* and 16*c*) for a fixed total sodium content ($x = 8$ was chosen).

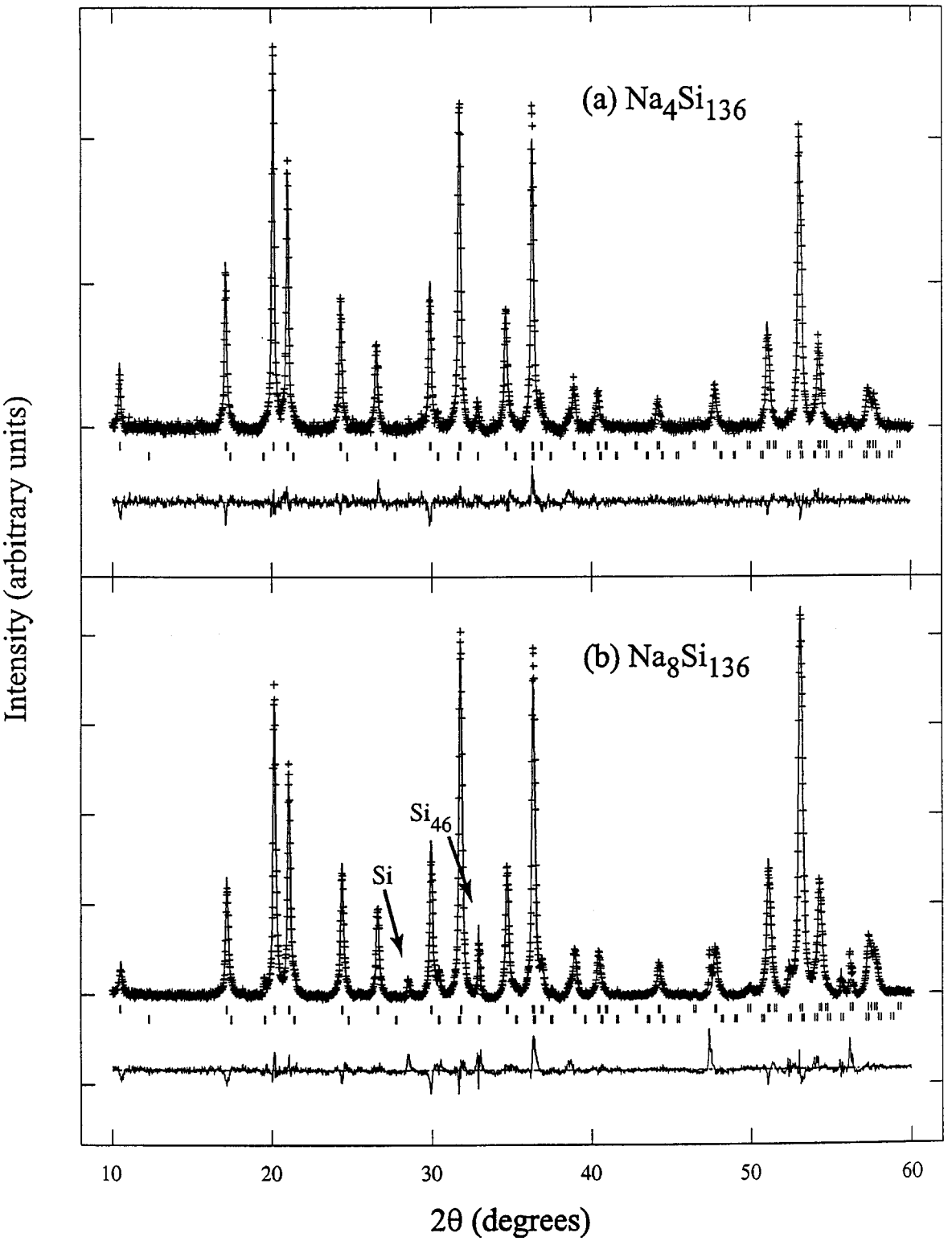

FIG. 7. Rietveld profile fits for (a) Na_4Si_{136} and (b) Na_8Si_{136} The sodium atom distribution in the two sites and the total sodium content were determined as revealed by the site occupancy of the 8*b* and 16*c* sites. Experimental data points are shown as plusses(+) and theoretical fits are shown as solid curves. The two sets of tick marks below each fit are the reflections corresponding to both Na_xSi_{136} (top) and the contaminant Na_8Si_{136} (bottom). Also shown below each fit is the difference between the observed and theoretical patterns. The sodium contents in Na_xSi_{136} have been rounded off to the nearest integer. See Tables 3 and 4 for details of the refinement. The sample of Na_8Si_{136} contained some elemental Si, and the peak as identified in the figure. The most intense reflection of Na_8Si_{46} is also shown.

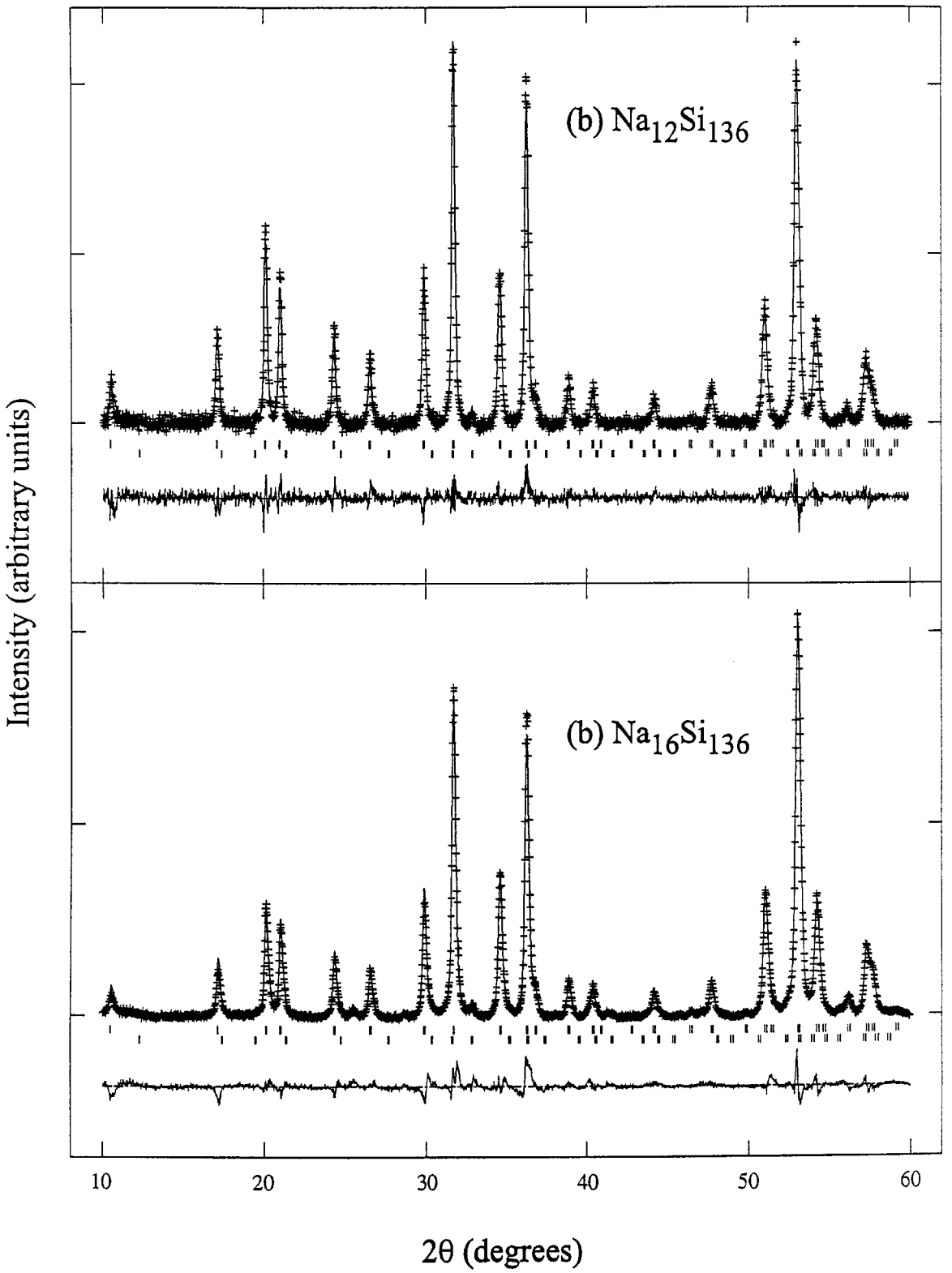

FIG. 8. Rietveld profile fits for (a) $Na_{12}Si_{136}$ and (b) $Na_{16}Si_{136}$. The sodium atom distribution in the two sites and the total sodium content were determined as revealed by the site occupancy of the 8*b* and 16*c* sites. Experimental data points are shown as plusses(+) and theoretical fits are shown as solid curves. The two sets of tick marks below each fit are the reflections corresponding to both Na_xSi_{136} (top) and the contaminant Na_8Si_{46} (bottom). Also shown below each fit is the difference between the observed and theoretical patterns. The sodium contents in Na_xSi_{136} have been rounded off to the nearest integer. See Tables 3 and 4 for details of the refinement.

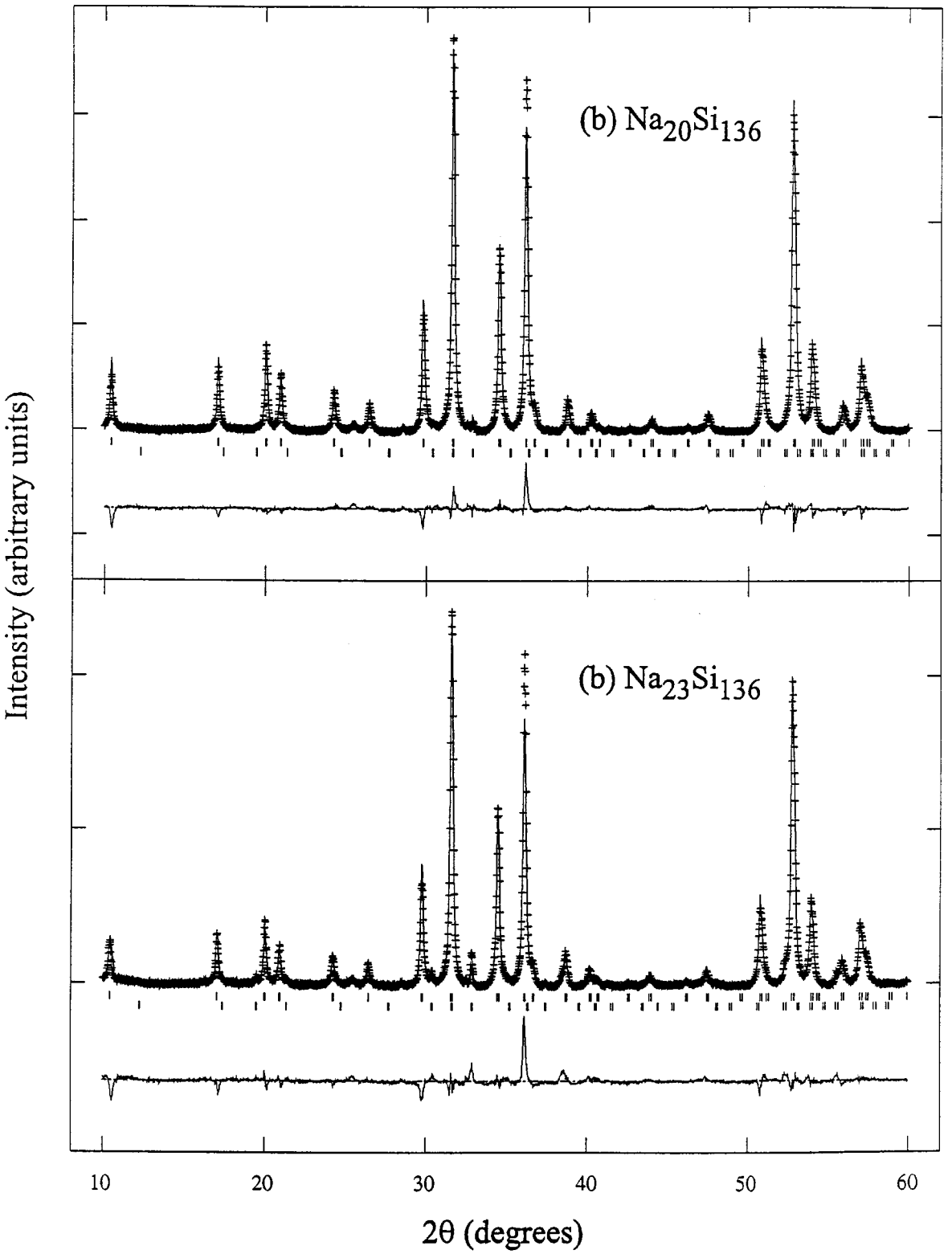

FIG. 9. Rietveld profile fits for (a) $Na_{20}Si_{136}$ and (b) $Na_{23}Si_{136}$. The sodium atom distribution in the two sites and the total sodium content were determined as revealed by the site occupancy of the 8*b* and 16*c* sites. Experimental data points are shown as plusses(+) and theoretical fits are shown as solid curves. The two sets of thick marks below each fit are the reflections corresponding to both Na_xSi_{136} (top) and the contaminant Na_8Si_{136} (bottom). Also shown below each fit is the difference between the observed and theoretical patterns. The sodium contents in Na_xSi_{136} have been rounded off to the nearest integer. See Tables 3 and 4 for details of the refinement.

TABLE 3
Atomic Positions, Site Occupancies, and Thermal Displacement Factors for Na_xSi_{136}

Atom	Site	x	y	z	Occupancy	100 U_{iso} (Å^2)
Na_4Si_{136} [Fig. 7a; $\chi^2 = 1.31$, $R_p = 0.057$, $R_{wp} = 0.074$; contained $\sim 3\%$ Na_8Si_{46}]						
Si1	8*a*	7/8	7/8	7/8	1.002(4)	4.40(4)
Si2	32*e*	0.7818(1)	0.7818(1)	0.7818(1)	0.995(3)	4.40(4)
Si3	96*g*	0.8168(1)	0.8168(1)	0.6288(1)	0.982(2)	4.40(4)
Na1	8*b*	3/8	3/8	3/8	0.473(6)	8.80(2)
Na2	16*c*	0	0	0	0.038(7)	9.13(2)
Na_8Si_{136} [Fig. 7b; $\chi^2 = 3.91$, $R_p = 0.044$, $R_{wp} = 0.065$; contained $\sim 9\%$ Na_8Si_{46}]						
Si1	8*a*	7/8	7/8	7/8	1.000(3)	1.38(1)
Si2	32*e*	0.7816(1)	0.7816(1)	0.7816(1)	0.985(6)	1.38(1)
Si3	96*g*	0.8166(1)	0.8166(1)	0.6288(1)	0.978(4)	1.38(1)
Na1	8*b*	3/8	3/8	3/8	0.721(5)	11.43(3)
Na2	16*c*	0	0	0	0.123(9)	9.00(2)
$Na_{12}Si_{136}$ [Fig. 8a; $\chi^2 = 1.51$, $R_p = 0.049$, $R_{wp} = 0.068$; contained $\sim 1\%$ Na_8Si_{46}]						
Si1	8*a*	7/8	7/8	7/8	1.012(8)	0.61(8)
Si2	32*e*	0.7815(2)	0.7815(2)	0.7815(2)	0.998(6)	0.61(8)
Si3	96*g*	0.8168(1)	0.8168(1)	0.6285(2)	0.987(4)	0.61(8)
Na1	8*b*	3/8	3/8	3/8	0.938(2)	10.00(2)
Na2	16*c*	0	0	0	0.307(4)	4.06(2)
$Na_{16}Si_{136}$ [Fig. 8b; $\chi^2 = 3.34$, $R_p = 0.052$, $R_{wp} = 0.067$; contained $\sim 1\%$ Na_8Si_{46}]						
Si1	8*a*	7/8	7/8	7/8	1.018(6)	1.998(5)
Si2	32*e*	0.7812(1)	0.7812(1)	0.7812(1)	0.993(4)	1.998(5)
Si3	96*g*	0.8167(1)	0.8167(1)	0.6284(1)	0.990(3)	1.998(5)
Na1	8*b*	3/8	3/8	3/8	0.971(8)	12.55(2)
Na2	16*c*	0	0	0	0.519(5)	3.43(1)
$Na_{20}Si_{136}$ [Fig. 9a; $\chi^2 = 3.51$, $R_p = 0.054$, $R_{wp} = 0.072$; contained $\sim 1\%$ Na_8Si_{46}]						
Si1	8*a*	7/8	7/8	7/8	0.992(5)	0.643(5)
Si2	32*e*	0.7808(1)	0.7808(1)	0.7808(1)	0.977(3)	0.643(5)
Si3	96*g*	0.8166(1)	0.8166(1)	0.6277(1)	0.995(2)	0.643(5)
Na1	8*b*	3/8	3/8	3/8	0.983(7)	14.15(2)
Na2	16*c*	0	0	0	0.781(4)	0.57(1)
$Na_{23}Si_{136}$ [Fig. 9b; $\chi^2 = 3.57$, $R_p = 0.054$, $R_{wp} = 0.071$; contained $\sim 2\%$ Na_8Si_{46}]						
Si1	8*a*	7/8	7/8	7/8	0.988(6)	0.211(6)
Si2	32*e*	0.7809(1)	0.7809(1)	0.7809(1)	0.971(2)	0.211(6)
Si3	96*g*	0.8166(1)	0.8166(1)	0.6277(1)	0.987(3)	0.211(6)
Na1	8*b*	3/8	3/8	3/8	0.998(5)	12.12(3)
Na2	16*c*	0	0	0	0.961(3)	0.44(3)

and

$$W = \frac{8N!}{m_1!(8N - m_1)!} \cdot \frac{8N!}{m_2!(8N - m_2)!}. \quad [1]$$

The condition $\delta A = 0$ requires that

$$\frac{\delta A}{\delta m_1} = -\frac{\delta A}{\delta m_2}. \quad [2]$$

Then setting

$$\varepsilon = E_{16c-\text{site}} - E_{8b-\text{site}} \quad [3]$$

as the energy difference between the two sites and solving Eqs. [1]–[3], we obtain, upon rearranging,

$$\frac{y_2(1 - y_1)}{y_1(1 - y_2)} = e^{-\varepsilon/kT}. \quad [4]$$

We also have

$$y_1 + 2y_2 = 3y. \quad [5]$$

Thus we can obtain $y_1(y)$ and $y_2(y)$ by solving Eqs. [4] and [5]. Of course, y_1 and y_2 are also functions of the parameter $\exp(-\varepsilon/kT)$. Figures 12a–d illustrate the change in the site occupation function as the parameter ε is varied, keeping the temperature constant at 375°C (~ 56 meV). When the energy difference between the two sites is very large ($\varepsilon \gg 1$ eV), the sodium atoms will occupy the energy stabilized cages until such cages are completely filled (Fig. 12a). In the other extreme case, when the two sites are equal in energy, the site occupancy function is linear in Na content (Fig. 12d). To estimate $\exp(-\varepsilon/kT)$, and subsequently ε, we fit our experimental data with Eq. [4] to obtain $\varepsilon = 0.190 \pm 0.050$ eV for the experimental synthesis temperature of 375°C; i.e., it is energetically more favorable to add Na atoms to the larger (8*b*) sites first. In the same spirit, sodium atoms from a sample of $Na_{24}Si_{136}$ will be preferentially *removed* from the smaller dodecahedral (16*c*) sites first, since the smaller cages are higher in energy. The underlying assumption that the energy difference ε does not vary with the total sodium content appears to be reasonable, given the excellent agreement between experiment and theory (Fig. 11), constrained by the experimental data at both low and high sodium contents.[1]

The argument that Na atoms at lower sodium contents preferentially occupy the larger sites is borne out by the observations of Cros *et al.* (1) on Cs-containing clathrates. Samples of Cs_xSi_{136} (maximum values of x obtained were 6 or 7) are never observed with full stoichiometry, due to the energy cost required for large Cs atoms to fit in the smaller cages. In the case of $Na_2Ba_6Si_{46}$, the smaller sodium atoms occupy the small cages and the larger barium atoms occupy the large cages (4).

[1]Data points at the extremes (occupancy of 0 and 1) were omitted since the form of the function in Eq. [4] diverges at these points.

TABLE 4[a]
Unit Cell Edges etc. for Na_xSi_{136}

Space group $Fd\bar{3}m$
Radiation wavelength Cu$K\alpha$ 1.5406 Å

Sample	Na content from X-ray analysis	a(Å)	V(Å^3)	$\rho_{X\text{-ray}}$ (g/cc)	ρ_{bulk} (g/cc)	Elemental analysis (weight %)
Na_4Si_{136}	4.394 ± 0.033	14.61963(1)	3124.71	2.056	2.040	Si 97.21 ± 2.35 Na 2.79 ± 2.00
Na_6Si_{136}	5.7584 ± 0.017	14.62202(1)	3126.24	2.078	2.050	—
Na_7Si_{136}	6.608 ± 0.032	14.63764(1)	3136.27	2.117	2.121	—
Na_8Si_{136}	7.737 ± 0.039	14.63101(2)	3132.01	2.109	2.191	Si 96.99 ± 2.11 Na 3.01 ± 2.12
$Na_{10}Si_{136}$	10.024 ± 0.017	14.64103(1)	3138.45	2.149	2.152	—
$Na_{10}Si_{136}$	10.152 ± 0.024	14.64094(2)	3138.39	2.133	2.153	—
$Na_{12}Si_{136}$	12.416 ± 0.017	14.64758(1)	3142.66	2.152	2.156	Si 92.93 ± 2.24 Na 7.07 ± 2.22
$Na_{12}Si_{136}$	12.432 ± 0.039	14.63687(3)	3135.77	2.179	2.193	—
$Na_{12}Si_{136}$	12.448 ± 0.017	14.64869(2)	3143.38	2.136	2.153	—
$Na_{13}Si_{136}$	13.016 ± 0.024	14.65783(3)	3149.26	2.117	2.233	—
$Na_{16}Si_{136}$	16.072 ± 0.030	14.66578(2)	3154.39	2.189	2.210	—
$Na_{18}Si_{136}$	17.728 ± 0.009	14.66723(3)	3155.33	2.278	2.273	—
$Na_{20}Si_{136}$	20.360 ± 0.025	14.68031(1)	3163.77	2.234	2.255	Si 89.79 ± 2.36 Na 10.21 ± 2.13
$Na_{21}Si_{136}$	21.144 ± 0.025	14.70620(1)	3180.59	2.321	2.281	—
$Na_{23}Si_{136}$	23.361 ± 0.018	14.70704(1)	3181.09	2.242	2.283	Si 87.43 ± 1.76 Na 12.57 ± 1.51

[a]Rietveld profile fits for compositions in bold ($x = 4, 8, 12, 16, 20, 23$) are shown in Figs. 7, 8, and 9. The others, along with fits and data, can be obtained from Supplementary Information.

CONCLUDING REMARKS

In conclusion, we have carefully examined the stoichiometry of the Na_8Si_{46} phase by chemical and Rietveld profile analysis of the X-ray powder diffraction data. We do not find any noticeable departures from the ideal stoichiometry in either the silicon framework or the endohedral sodium atoms. In the Na_xSi_{136} series, the silicon framework maintains stoichiometry, but the sodium concentrations vary. Identification and estimation of the total sodium content and Na site occupancy in Na_xSi_{136} clathrate phase are readily achieved by visual inspection of the X-ray powder diffraction pattern. This is useful for rapid assessment of sample quality. The Na content and site distribution were refined by Rietveld profile analysis and are in good agreement with chemical analysis and bulk density measurements. In the same structure, a 0.5% expansion in the unit cell edge is observed upon progressing from Na_4Si_{136} to $Na_{23}Si_{136}$. At 375°C, the synthesis temperature of our Na_xSi_{136} samples, it is shown that the removal of sodium atoms from the smaller dodecahedra (Si_{20}) is preferred over removal from the larger hexakaidecahedra (Si_{28}) by 0.190 ± 0.05 eV.

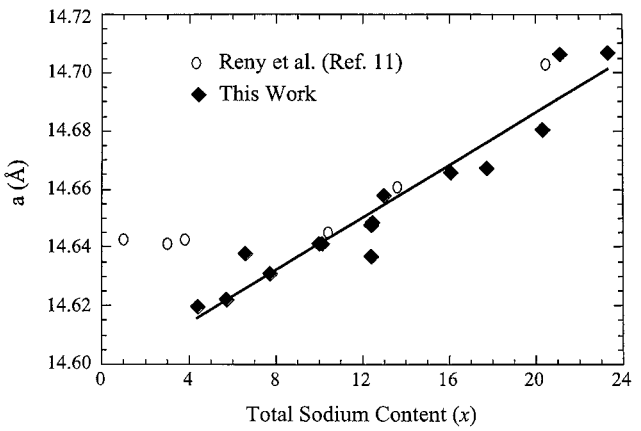

FIG. 10. Effect on unit cell edge "a" upon progressing from Na_4Si_{136} to $Na_{23}Si_{136}$. The expansion is approximately 0.5%. Open circles are data from a very recent report by Reny *et al.* [11]. The filled diamonds are data from this work (see the section on Na_xSi_{136}). The solid least-squares curve is an eye guide.

SUPPLEMENTARY INFORMATION

Additional data for all samples (of Na_xSi_{136}) discussed but not presented in this text can be obtained from Tables

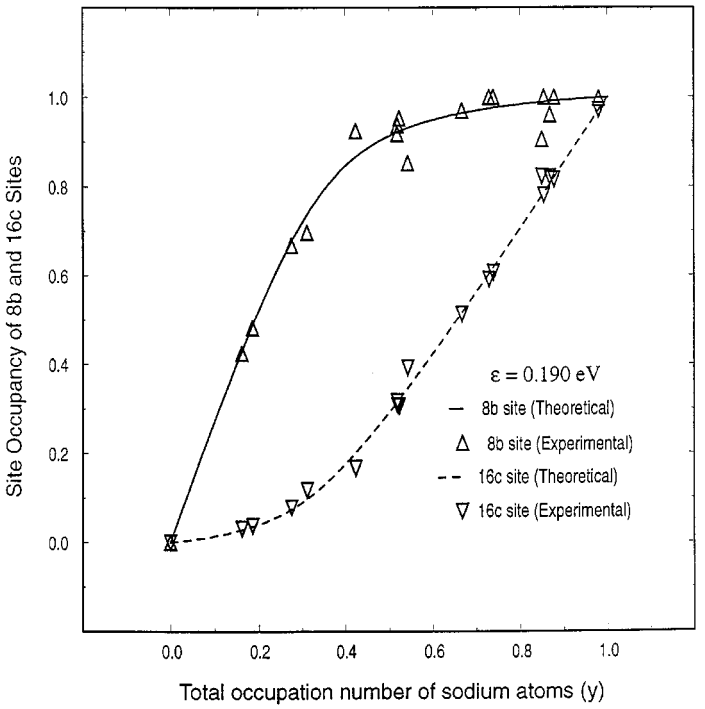

FIG. 11. The sodium atoms preferentially occupy the larger hexakaidecahedral cages in the Na_xSi_{136} structure; plotted are the experimental data of site occupancies for hexakaidecahedral (8*b*, upright triangles) and dodecahedral (16*c*, inverted triangles) sites in Na_xSi_{136} as a function of total sodium content. The *x*-axis is normalized to 1, corresponding to a fully loaded sample with $x = 24$. The theoretical fits shown in solid (8*b* sites) and broken lines (16*c* sites) reveal a preference for the addition of sodium to the larger (hexakaidecahedra, 8*b* sites) cages than to the smaller cages (dodecahedra, 16*c* sites) by 0.190 ± 0.050 eV. Site occupancy data for Na_0Si_{136} and $Na_{24}Si_{136}$ were incorporated along with the experimental data.

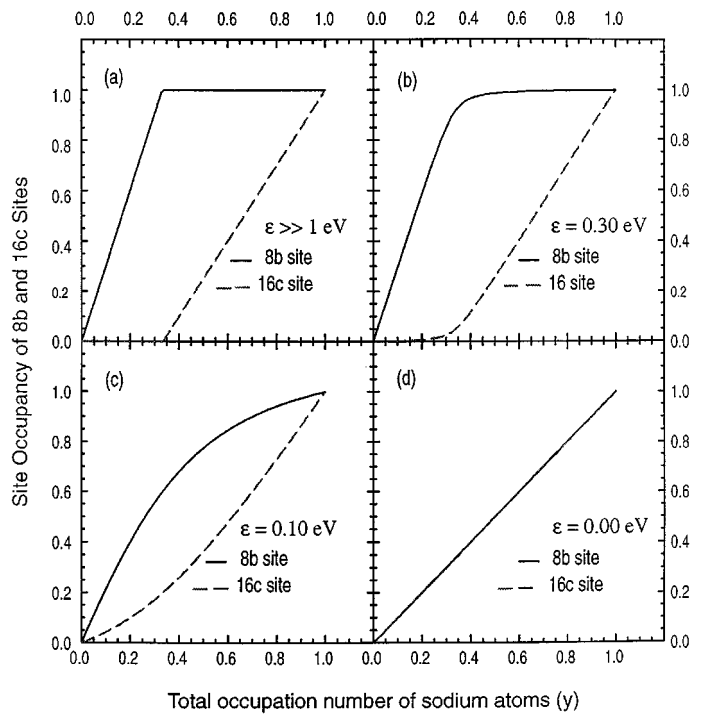

FIG. 12. The effect of an energy difference (ε) for the addition of sodium to the small and large cages in the Na_xSi_{136} structure: (a) when the energy difference between the two sites is very large ($\varepsilon \gg 1$ eV), the sodium atoms will fill all the energy stabilized (hexakaidecahedra, 8*b* sites) cages until there are no such available. (d) In the other extreme case, when the energy difference between either site is equal, the site occupancy function is linear in Na content. Depicted in (b) and (c) are the filling scheme for intermediate energy differences.

1 through 4 and Figs. 1 through 4 of Supplementary Information.[2] Table 5 contains data on Na_8Si_{46}, without constraints on thermal parameters.

ACKNOWLEDGMENTS

We are indebted to Professor Michael O'Keeffe for many valuable discussions and his insightful comments. Thanks are also due to Kurt Lienenweber and Michael Shemkunas for useful discussions. It is also our pleasure to thank one of the anonymous reviewers whose comments and suggestions helped shape the final form of this manuscript. This work was supported by NSF MRSEC award DMR 96-32635 and NSF award EAR 93-05425. A Jacksonville State University Faculty Research grant also supported one of us (J.G.).

REFERENCES

1. J. S. Kasper, P. Hagenmuller, M. Pouchard, and C. Cros, *Science* **150,** 1713 (1965). [C. Cros, M. Pouchard, and P. Hagenmuller, *C. R. Acad. Sc.* **260,** 4764 (1965); C. Cros, M. Pouchard, P. Hagenmuller, and J. S. Kasper, *Bull. Soc. Chim. France* **7,** 2737 (1968); C. Cros, M. Pouchard, and P. Hagenmuller, *J. Solid State Chem.* **2,** 570 (1970)].
2. G. A. Jeffrey, "Inclusion Compounds, Vol. I" (J. L. Atwood, J. E. D. Davies, and D. D. MacNicol, Eds.), p. 135. Academic Press, London, 1984. ["Molecular Inclusions and Molecular Recognition-Clathrates I," (R. Gerdil and E. Weber, Eds.), Topics in Current Chemistry, **140**. Springer-Verlag, Berlin, 1987; "Molecular Inclusions and Molecular Recognition-Clathrates II," (E. Weber and R. Bishop, Eds.), Topics in Current Chemistry, **149**. Springer-Verlag, Berlin, 1988].
3. G. B. Adams, M. O'Keeffe, A. A. Demkov, O. F. Sankey, and Y. Huang, *Phys. Rev. B* **49,** 8048 (1994). [A. A. Demkov, O. F. Sankey, K. E. Schmidt, G. B. Adams, and M. O'Keeffe, *Phys. Rev. B* **50,** 17001 (1994)].
4. H. Kawaji, H. Horie, H. Nakano, and M. Ishikawa, *Phys. Rev. Lett.* **74,** 1427 (1995). [S. Saito and A. Oshiyama, *Phys. Rev. B* **51,** 2628 (1995); S. Yamanaka, H. Horie, H. Nakano, and M. Ishikawa, *Fullerene Sci. Tech.* **3,** 21 (1995)]
5. A. F. Hebard, M. J. Rosseinsky, R. C. Haddon, D. W. Murphy, S. H. Glarum, T. T. M. Palstra, A. P. Ramirez, and A. R. Kortan, *Nature* **350,** 600 (1991).
6. N. F. Mott, *J. Solid State Chem.* **6,** 348 (1973).
7. R. F. W. Herrmann, K. Tanigaki, S. Kuroshima, and H. Suematsu, *Chem. Phys. Lett.* **283,** 29 (1998).
8. G. Nolas, J. L. Cohn, G. A. Slack, and S. B. Schujman, *Appl. Phys. Lett.* **73,** 178 (1998). [G. A. Slack, *Mat. Res. Soc. Symp. Proc.* **478,** 47 (1997); J. Dong, O. F. Sankey, A. A. Demkov, G. K. Ramachandran, J. Gryko, P. F. McMillan, and W. Windl, *Mat. Res. Soc. Symp. Proc.* **545** (1999); G. S. Nolas, private communication]
9. J-T. Zhao and J. D. Corbett, *Inorg. Chem.* **33,** 5721 (1994). ["Chemistry, Structure and Bonding of Zintl Phases and Ions ed. (S. M. Kauzlarich, Ed.), pp. 23, 141. VCH, New York, 1996].
10. S. B. Roy, K. E. Sim, and A. D. Caplin, *Philos. Mag. B* **65,** 1445 (1992).
11. E. Reny, P. Gravereau, C. Cros, and M. Pouchard, *J. Mater. Chem.* **8,** 2839 (1998).
12. A. C. Larson and R. B. von Dreele, "GSAS Generalized Structure Analysis System," LANSCE, MS-H805, Manual Lujan Neutron Scattering Center, Los Alamos, NM, 1989.
13. G. K. Ramachandran, J. Diefenbacher, J. Dong, J. Gryko, O. F. Sankey, and P. F. McMillan, Submitted.

[2]See NAPS document No. 05517 for 12 pages of supplementary material. This is not a multi-article document. Order from NAPS c/o Microfiche Publications, 248 Hempstead Turnpike, West Hempstead, New York 11552. Remit in advance in U.S. funds only $15.00 for photocopies or $5.00 for microfiche. There is a $25.00 invoicing charge on all orders filled before payment. Outside U.S. and Canada add postage of $4.50 for the first 20 pages and $1.00 for each 10 pages of material thereafter, or $5.00 for the first microfiche and $1.00 for each fiche thereafter.